

Measurement of the Forward-Backward Asymmetry in the Production of B^\pm Mesons in $p\bar{p}$ Collisions at $\sqrt{s} = 1.96$ TeV

V. M. Abazov,³¹ B. Abbott,⁶⁷ B. S. Acharya,²⁵ M. Adams,⁴⁶ T. Adams,⁴⁴ J. P. Agnew,⁴¹ G. D. Alexeev,³¹ G. Alkhazov,³⁵ A. Alton,^{56,a} A. Askew,⁴⁴ S. Atkins,⁵⁴ K. Augsten,⁷ C. Avila,⁵ F. Badaud,¹⁰ L. Bagby,⁴⁵ B. Baldin,⁴⁵ D. V. Bandurin,⁷³ S. Banerjee,²⁵ E. Barberis,⁵⁵ P. Baringer,⁵³ J. F. Bartlett,⁴⁵ U. Bassler,¹⁵ V. Bazterra,⁴⁶ A. Bean,⁵³ M. Begalli,² L. Bellantoni,⁴⁵ S. B. Beri,²³ G. Bernardi,¹⁴ R. Bernhard,¹⁹ I. Bertram,³⁹ M. Besançon,¹⁵ R. Beuselinck,⁴⁰ P. C. Bhat,⁴⁵ S. Bhatia,⁵⁸ V. Bhatnagar,²³ G. Blazey,⁴⁷ S. Blessing,⁴⁴ K. Bloom,⁵⁹ A. Boehnlein,⁴⁵ D. Boline,⁶⁴ E. E. Boos,³³ G. Borissov,³⁹ M. Borysova,^{38,l} A. Brandt,⁷⁰ O. Brandt,²⁰ R. Brock,⁵⁷ A. Bross,⁴⁵ D. Brown,¹⁴ X. B. Bu,⁴⁵ M. Buehler,⁴⁵ V. Buescher,²¹ V. Bunichev,³³ S. Burdin,^{39,b} C. P. Buszello,³⁷ E. Camacho-Pérez,²⁸ B. C. K. Casey,⁴⁵ H. Castilla-Valdez,²⁸ S. Caughron,⁵⁷ S. Chakrabarti,⁶⁴ K. M. Chan,⁵¹ A. Chandra,⁷² E. Chapon,¹⁵ G. Chen,⁵³ S. W. Cho,²⁷ S. Choi,²⁷ B. Choudhary,²⁴ S. Cihangir,⁴⁵ D. Claes,⁵⁹ J. Clutter,⁵³ M. Cooke,^{45,k} W. E. Cooper,⁴⁵ M. Corcoran,⁷² F. Couderc,¹⁵ M.-C. Cousinou,¹² D. Cutts,⁶⁹ A. Das,⁴² G. Davies,⁴⁰ S. J. de Jong,^{29,30} E. De La Cruz-Burelo,²⁸ F. Déliot,¹⁵ R. Demina,⁶³ D. Denisov,⁴⁵ S. P. Denisov,³⁴ S. Desai,⁴⁵ C. Deterre,^{41,c} K. DeVaughan,⁵⁹ H. T. Diehl,⁴⁵ M. Diesburg,⁴⁵ P. F. Ding,⁴¹ A. Dominguez,⁵⁹ A. Dubey,²⁴ L. V. Dudko,³³ A. Duperrin,¹² S. Dutt,²³ M. Eads,⁴⁷ D. Edmunds,⁵⁷ J. Ellison,⁴³ V. D. Elvira,⁴⁵ Y. Enari,¹⁴ H. Evans,⁴⁹ V. N. Evdokimov,³⁴ A. Fauré,¹⁵ L. Feng,⁴⁷ T. Ferbel,⁶³ F. Fiedler,²¹ F. Filthaut,^{29,30} W. Fisher,⁵⁷ H. E. Fisk,⁴⁵ M. Fortner,⁴⁷ H. Fox,³⁹ S. Fuess,⁴⁵ P. H. Garbincius,⁴⁵ A. Garcia-Bellido,⁶³ J. A. García-González,²⁸ V. Gavrilov,³² W. Geng,^{12,57} C. E. Gerber,⁴⁶ Y. Gershtein,⁶⁰ G. Ginther,^{45,63} O. Gogota,³⁸ G. Golovanov,³¹ P. D. Grannis,⁶⁴ S. Greder,¹⁶ H. Greenlee,⁴⁵ G. Grenier,¹⁷ Ph. Gris,¹⁰ J.-F. Grivaz,¹³ A. Grohsjean,^{15,c} S. Grünendahl,⁴⁵ M. W. Grünewald,²⁶ T. Guillemain,¹³ G. Gutierrez,⁴⁵ P. Gutierrez,⁶⁷ J. Haley,⁶⁸ L. Han,⁴ K. Harder,⁴¹ A. Harel,⁶³ J. M. Hauptman,⁵² J. Hays,⁴⁰ T. Head,⁴¹ T. Hebbeker,¹⁸ D. Hedin,⁴⁷ H. Hegab,⁶⁸ A. P. Heinson,⁴³ U. Heintz,⁶⁹ C. Hensel,¹ I. Heredia-De La Cruz,^{28,d} K. Herner,⁴⁵ G. Hesketh,^{41,f} M. D. Hildreth,⁵¹ R. Hirosky,⁷³ T. Hoang,⁴⁴ J. D. Hobbs,⁶⁴ B. Hoeneisen,⁹ J. Hogan,⁷² M. Hohlfield,²¹ J. L. Holzbauer,⁵⁸ I. Howley,⁷⁰ Z. Hubacek,^{7,15} V. Hynek,⁷ I. Iashvili,⁶² Y. Ilchenko,⁷¹ R. Illingworth,⁴⁵ A. S. Ito,⁴⁵ S. Jabeen,^{45,m} M. Jaffré,¹³ A. Jayasinghe,⁶⁷ M. S. Jeong,²⁷ R. Jesik,⁴⁰ P. Jiang,⁴ K. Johns,⁴² E. Johnson,⁵⁷ M. Johnson,⁴⁵ A. Jonckheere,⁴⁵ P. Jonsson,⁴⁰ J. Joshi,⁴³ A. W. Jung,⁴⁵ A. Juste,³⁶ E. Kajfasz,¹² D. Karmanov,³³ I. Katsanos,⁵⁹ M. Kaur,²³ R. Kehoe,⁷¹ S. Kermiche,¹² N. Khalatyan,⁴⁵ A. Khanov,⁶⁸ A. Kharchilava,⁶² Y. N. Kharzheev,³¹ I. Kiselevich,³² J. M. Kohli,²³ A. V. Kozelov,³⁴ J. Kraus,⁵⁸ A. Kumar,⁶² A. Kupco,⁸ T. Kurča,¹⁷ V. A. Kuzmin,³³ S. Lammers,⁴⁹ P. Lebrun,¹⁷ H. S. Lee,²⁷ S. W. Lee,⁵² W. M. Lee,⁴⁵ X. Lei,⁴² J. Lellouch,¹⁴ D. Li,¹⁴ H. Li,⁷³ L. Li,⁴³ Q. Z. Li,⁴⁵ J. K. Lim,²⁷ D. Lincoln,⁴⁵ J. Linnemann,⁵⁷ V. V. Lipaev,³⁴ R. Lipton,⁴⁵ H. Liu,⁷¹ Y. Liu,⁴ A. Lobodenko,³⁵ M. Lokajicek,⁸ R. Lopes de Sa,⁴⁵ R. Luna-Garcia,^{28,g} A. L. Lyon,⁴⁵ A. K. A. Maciel,¹ R. Madar,¹⁹ R. Magaña-Villalba,²⁸ S. Malik,⁵⁹ V. L. Malyshev,³¹ J. Mansour,²⁰ J. Martínez-Ortega,²⁸ R. McCarthy,⁶⁴ C. L. McGivern,⁴¹ M. M. Meijer,^{29,30} A. Melnitchouk,⁴⁵ D. Menezes,⁴⁷ P. G. Mercadante,³ M. Merkin,³³ A. Meyer,¹⁸ J. Meyer,^{20,i} F. Miconi,¹⁶ N. K. Mondal,²⁵ M. Mulhearn,⁷³ E. Nagy,¹² M. Narain,⁶⁹ R. Nayyar,⁴² H. A. Neal,⁵⁶ J. P. Negret,⁵ P. Neustroev,³⁵ H. T. Nguyen,⁷³ T. Nunnemann,²² J. Orduna,⁷² N. Osman,¹² J. Osta,⁵¹ A. Pal,⁷⁰ N. Parashar,⁵⁰ V. Parihar,⁶⁹ S. K. Park,²⁷ R. Partridge,^{69,e} N. Parua,⁴⁹ A. Patwa,^{65,j} B. Penning,⁴⁵ M. Perfilov,³³ Y. Peters,⁴¹ K. Petridis,⁴¹ G. Petrillo,⁶³ P. Pétrouff,¹³ M.-A. Pleier,⁶⁵ V. M. Podstavkov,⁴⁵ A. V. Popov,³⁴ M. Prewitt,⁷² D. Price,⁴¹ N. Prokopenko,³⁴ J. Qian,⁵⁶ A. Quadt,²⁰ B. Quinn,⁵⁸ P. N. Ratoff,³⁹ I. Razumov,³⁴ I. Ripp-Baudot,¹⁶ F. Rizatdinova,⁶⁸ M. Rominsky,⁴⁵ A. Ross,³⁹ C. Royon,¹⁵ P. Rubinov,⁴⁵ R. Ruchti,⁵¹ G. Sajot,¹¹ A. Sánchez-Hernández,²⁸ M. P. Sanders,²² A. S. Santos,^{1,h} G. Savage,⁴⁵ M. Savitskiy,³⁸ L. Sawyer,⁵⁴ T. Scanlon,⁴⁰ R. D. Schamberger,⁶⁴ Y. Scheglov,³⁵ H. Schellman,⁴⁸ C. Schwanenberger,⁴¹ R. Schwienhorst,⁵⁷ J. Sekaric,⁵³ H. Severini,⁶⁷ E. Shabalina,²⁰ V. Shary,¹⁵ S. Shaw,⁴¹ A. A. Shchukin,³⁴ V. Simak,⁷ P. Skubic,⁶⁷ P. Slattery,⁶³ D. Smirnov,⁵¹ G. R. Snow,⁵⁹ J. Snow,⁶⁶ S. Snyder,⁶⁵ S. Söldner-Rembold,⁴¹ L. Sonnenschein,¹⁸ K. Soustruznik,⁶ J. Stark,¹¹ D. A. Stoyanova,³⁴ M. Strauss,⁶⁷ L. Suter,⁴¹ P. Svoisky,⁶⁷ M. Titov,¹⁵ V. V. Tokmenin,³¹ Y.-T. Tsai,⁶³ D. Tsybychev,⁶⁴ B. Tuchming,¹⁵ C. Tully,⁶¹ L. Uvarov,³⁵ S. Uvarov,³⁵ S. Uzunyan,⁴⁷ R. Van Kooten,⁴⁹ W. M. van Leeuwen,²⁹ N. Varelas,⁴⁶ E. W. Varnes,⁴² I. A. Vasilyev,³⁴ A. Y. Verkheev,³¹ L. S. Vertogradov,³¹ M. Verzocchi,⁴⁵ M. Vesterinen,⁴¹ D. Vilanova,¹⁵ P. Vokac,⁷ H. D. Wahl,⁴⁴ M. H. L. S. Wang,⁴⁵ J. Warchol,⁵¹ G. Watts,⁷⁴ M. Wayne,⁵¹ J. Weichert,²¹ L. Welty-Rieger,⁴⁸ M. R. J. Williams,^{49,n} G. W. Wilson,⁵³ M. Wobisch,⁵⁴ D. R. Wood,⁵⁵ T. R. Wyatt,⁴¹ Y. Xie,⁴⁵ R. Yamada,⁴⁵ S. Yang,⁴ T. Yasuda,⁴⁵ Y. A. Yatsunenkov,³¹ W. Ye,⁶⁴ Z. Ye,⁴⁵ H. Yin,⁴⁵ K. Yip,⁶⁵ S. W. Youn,⁴⁵ J. M. Yu,⁵⁶ J. Zennamo,⁶² T. G. Zhao,⁴¹ B. Zhou,⁵⁶ J. Zhu,⁵⁶ M. Zielinski,⁶³ D. Zieminska,⁴⁹ and L. Zivkovic¹⁴

(D0 Collaboration)

- ¹LAFEX, Centro Brasileiro de Pesquisas Físicas, Rio de Janeiro, Brazil
²Universidade do Estado do Rio de Janeiro, Rio de Janeiro, Brazil
³Universidade Federal do ABC, Santo André, Brazil
⁴University of Science and Technology of China, Hefei, People's Republic of China
⁵Universidad de los Andes, Bogotá, Colombia
⁶Charles University, Faculty of Mathematics and Physics, Center for Particle Physics, Prague, Czech Republic
⁷Czech Technical University in Prague, Prague, Czech Republic
⁸Institute of Physics, Academy of Sciences of the Czech Republic, Prague, Czech Republic
⁹Universidad San Francisco de Quito, Quito, Ecuador
¹⁰LPC, Université Blaise Pascal, CNRS/IN2P3, Clermont, France
¹¹LPSC, Université Joseph Fourier Grenoble 1, CNRS/IN2P3, Institut National Polytechnique de Grenoble, Grenoble, France
¹²CPPM, Aix-Marseille Université, CNRS/IN2P3, Marseille, France
¹³LAL, Université Paris-Sud, CNRS/IN2P3, Orsay, France
¹⁴LPNHE, Universités Paris VI and VII, CNRS/IN2P3, Paris, France
¹⁵CEA, Irfu, SPP, Saclay, France
¹⁶IPHC, Université de Strasbourg, CNRS/IN2P3, Strasbourg, France
¹⁷IPNL, Université Lyon 1, CNRS/IN2P3, Villeurbanne, France and Université de Lyon, Lyon, France
¹⁸III. Physikalisches Institut A, RWTH Aachen University, Aachen, Germany
¹⁹Physikalisches Institut, Universität Freiburg, Freiburg, Germany
²⁰II. Physikalisches Institut, Georg-August-Universität Göttingen, Göttingen, Germany
²¹Institut für Physik, Universität Mainz, Mainz, Germany
²²Ludwig-Maximilians-Universität München, München, Germany
²³Panjab University, Chandigarh, India
²⁴Delhi University, Delhi, India
²⁵Tata Institute of Fundamental Research, Mumbai, India
²⁶University College Dublin, Dublin, Ireland
²⁷Korea Detector Laboratory, Korea University, Seoul, Korea
²⁸CINVESTAV, Mexico City, Mexico
²⁹Nikhef, Science Park, Amsterdam, the Netherlands
³⁰Radboud University Nijmegen, Nijmegen, the Netherlands
³¹Joint Institute for Nuclear Research, Dubna, Russia
³²Institute for Theoretical and Experimental Physics, Moscow, Russia
³³Moscow State University, Moscow, Russia
³⁴Institute for High Energy Physics, Protvino, Russia
³⁵Petersburg Nuclear Physics Institute, St. Petersburg, Russia
³⁶Institució Catalana de Recerca i Estudis Avançats (ICREA) and Institut de Física d'Altes Energies (IFAE), Barcelona, Spain
³⁷Uppsala University, Uppsala, Sweden
³⁸Taras Shevchenko National University of Kyiv, Kiev, Ukraine
³⁹Lancaster University, Lancaster LA1 4YB, United Kingdom
⁴⁰Imperial College London, London SW7 2AZ, United Kingdom
⁴¹The University of Manchester, Manchester M13 9PL, United Kingdom
⁴²University of Arizona, Tucson, Arizona 85721, USA
⁴³University of California Riverside, Riverside, California 92521, USA
⁴⁴Florida State University, Tallahassee, Florida 32306, USA
⁴⁵Fermi National Accelerator Laboratory, Batavia, Illinois 60510, USA
⁴⁶University of Illinois at Chicago, Chicago, Illinois 60607, USA
⁴⁷Northern Illinois University, DeKalb, Illinois 60115, USA
⁴⁸Northwestern University, Evanston, Illinois 60208, USA
⁴⁹Indiana University, Bloomington, Indiana 47405, USA
⁵⁰Purdue University Calumet, Hammond, Indiana 46323, USA
⁵¹University of Notre Dame, Notre Dame, Indiana 46556, USA
⁵²Iowa State University, Ames, Iowa 50011, USA
⁵³University of Kansas, Lawrence, Kansas 66045, USA
⁵⁴Louisiana Tech University, Ruston, Louisiana 71272, USA
⁵⁵Northeastern University, Boston, Massachusetts 02115, USA
⁵⁶University of Michigan, Ann Arbor, Michigan 48109, USA
⁵⁷Michigan State University, East Lansing, Michigan 48824, USA
⁵⁸University of Mississippi, University, Mississippi 38677, USA
⁵⁹University of Nebraska, Lincoln, Nebraska 68588, USA
⁶⁰Rutgers University, Piscataway, New Jersey 08855, USA

- ⁶¹Princeton University, Princeton, New Jersey 08544, USA
⁶²State University of New York, Buffalo, New York 14260, USA
⁶³University of Rochester, Rochester, New York 14627, USA
⁶⁴State University of New York, Stony Brook, New York 11794, USA
⁶⁵Brookhaven National Laboratory, Upton, New York 11973, USA
⁶⁶Langston University, Langston, Oklahoma 73050, USA
⁶⁷University of Oklahoma, Norman, Oklahoma 73019, USA
⁶⁸Oklahoma State University, Stillwater, Oklahoma 74078, USA
⁶⁹Brown University, Providence, Rhode Island 02912, USA
⁷⁰University of Texas, Arlington, Texas 76019, USA
⁷¹Southern Methodist University, Dallas, Texas 75275, USA
⁷²Rice University, Houston, Texas 77005, USA
⁷³University of Virginia, Charlottesville, Virginia 22904, USA
⁷⁴University of Washington, Seattle, Washington 98195, USA
(Received 13 November 2014; published 4 February 2015)

We present a measurement of the forward-backward asymmetry in the production of B^\pm mesons, $A_{\text{FB}}(B^\pm)$, using $B^\pm \rightarrow J/\psi K^\pm$ decays in 10.4 fb^{-1} of $p\bar{p}$ collisions at $\sqrt{s} = 1.96 \text{ TeV}$ collected by the D0 experiment during Run II of the Tevatron collider. A nonzero asymmetry would indicate a preference for a particular flavor, i.e., b quark or \bar{b} antiquark, to be produced in the direction of the proton beam. We extract $A_{\text{FB}}(B^\pm)$ from a maximum likelihood fit to the difference between the numbers of forward- and backward-produced B^\pm mesons. We measure an asymmetry consistent with zero: $A_{\text{FB}}(B^\pm) = [-0.24 \pm 0.41 \text{ (stat)} \pm 0.19 \text{ (syst)}]\%$.

DOI: [10.1103/PhysRevLett.114.051803](https://doi.org/10.1103/PhysRevLett.114.051803)

PACS numbers: 13.25.Hw, 11.30.Er

Over the past few years there has been much interest in the forward-backward asymmetry in $t\bar{t}$ production ($A_{\text{FB}}^{t\bar{t}}$) [1], especially since initial experimental results were larger than standard model (SM) predictions [2,3]. These observations prompted development of models beyond the SM that could explain the excess [4]. The corresponding asymmetry in $b\bar{b}$ production, $A_{\text{FB}}^{b\bar{b}}$, has the same sources as $A_{\text{FB}}^{t\bar{t}}$ but is expected to have a smaller magnitude in the SM, making it an important probe of these new physics models [5,6].

The most recent D0 measurements of $A_{\text{FB}}^{t\bar{t}}$ [7] agree with the SM [8]. A closely related quantity called the $t\bar{t}$ charge asymmetry has been studied at the LHC [9,10]. The LHCb collaboration has recently measured the charge asymmetry between b and \bar{b} jets in pp collisions [11].

A forward-backward asymmetry in the production of heavy quark Q is primarily caused by interference between tree-level and loop diagrams for $q\bar{q} \rightarrow Q\bar{Q}$ interactions, and also by interference between initial and final state gluon radiation [12]. We measure the forward-backward asymmetry using fully reconstructed $B^\pm \rightarrow J/\psi(\rightarrow \mu^+\mu^-)K^\pm$ decays where the B^\pm directly identifies the quark flavor (i.e., b or \bar{b}). Compared to b jet reconstruction, this method has the advantages that the charge of the b quark is unambiguously determined, and there is no need to account for B^0/\bar{B}^0 oscillations. The quantity $A_{\text{FB}}(B^\pm)$ is sensitive to the same production asymmetries as $A_{\text{FB}}^{b\bar{b}}$. In $p\bar{p}$ collisions, the forward category indicates a $b(\bar{b})$ quark, or $B^-(B^+)$ meson, emitted with a longitudinal momentum component in the direction of the proton (antiproton) beam.

We reconstruct a B^\pm meson and categorize it as forward or backward with a variable $q_{\text{FB}} = -q_B \text{sgn}(\eta_B)$, where q_B is the B^\pm meson electric charge, $\text{sgn}(x)$ is the sign function, and η_B is the B^\pm meson pseudorapidity [13]. The forward-backward asymmetry of the B^\pm mesons is

$$A_{\text{FB}}(B^\pm) = \frac{N(q_{\text{FB}} > 0) - N(q_{\text{FB}} < 0)}{N(q_{\text{FB}} > 0) + N(q_{\text{FB}} < 0)}. \quad (1)$$

Inclusive predictions of $A_{\text{FB}}^{b\bar{b}}$ give positive asymmetries of $\approx 0.5\%$ [5,14], but the mass scales of the $b\bar{b}$ pairs considered [$M(b\bar{b}) > 35 \text{ GeV}$, or $p(b) > \approx 15 \text{ GeV}$] are more relevant for a jet-based analysis. To make SM predictions tailored to our kinematics and selections, we produce next-to-leading-order Monte Carlo (MC) samples for QCD production of B^\pm in the process $p\bar{p} \rightarrow b\bar{b}X$. MC events are generated using MC@NLO [15] with parton distribution function (PDF) set CTEQ6M1 [16] and HERWIG [17] for parton showering and hadronization. Detector simulation is performed using GEANT3 [18].

The D0 experiment collected data at $\sqrt{s} = 1.96 \text{ TeV}$ during Run II of the Fermilab Tevatron $p\bar{p}$ collider, from 2002 until the Tevatron shutdown in 2011. The D0 detector is described in detail elsewhere [19]. For this analysis, the most important detector elements are the central tracking and muon systems. The central tracking system consists of a silicon microstrip tracker and a central fiber tracker, both located within a 1.9 T superconducting solenoidal magnet, with designs optimized for tracking and vertex finding at pseudorapidities $|\eta| < 3$ and $|\eta| < 2.5$, respectively.

The muon system has a layer of tracking detectors and scintillation trigger counters outside a liquid argon sampling calorimeter and two similar layers outside a 1.8 T iron toroid [20], and covers the region $|\eta_{\text{det}}| \approx 2$ where $|\eta_{\text{det}}|$ is measured from the center of the detector. The solenoid and toroid magnet polarities were reversed approximately every two weeks giving nearly equal beam exposure to each polarity combination. The data used in this analysis were collected with a suite of single muon and dimuon triggers.

We select $B^\pm \rightarrow J/\psi K^\pm$ candidates from the D0 Run II data set with an integrated luminosity of 10.4 fb^{-1} . Candidates are reconstructed by identifying a pair of oppositely charged muons (decay products of the J/ψ meson) produced along with a charged track (the K^\pm candidate) at a common vertex displaced from the $p\bar{p}$ interaction vertex.

All tracks must lie within the pseudorapidity coverage of the muon and central tracking systems, $|\eta| < 2.1$. Selected muons have transverse momentum $p_T > 1.5 \text{ GeV}$, and K^\pm candidates have $p_T > 0.7 \text{ GeV}$. At least one muon must traverse both inner and outer layers of the muon detector. Both muons must match to tracks in the central tracking system. The J/ψ candidates with reconstructed invariant mass $M(\mu^+\mu^-)$ between 2.7 and 3.45 GeV are accepted if their transverse decay length (L_{xy}) uncertainty is less than 0.1 cm, where L_{xy} is the distance from the $p\bar{p}$ vertex to a particle's decay vertex in the x - y plane. The cosine of the pointing angle [21] must be greater than zero.

The combination of μ^+ , μ^- , and K^\pm tracks to form a B^\pm decay vertex must have $\chi^2 < 16$ for 3 degrees of freedom, and the cosine of the B^\pm pointing angle must be above 0.8. B^\pm candidates are accepted if they are significantly displaced from the $p\bar{p}$ vertex. Their transverse decay length significance (defined as L_{xy} divided by its uncertainty) must be greater than three. To calculate the B^\pm candidate mass we correct the muon momenta by constraining $M(\mu^+\mu^-)$ to the world average J/ψ meson mass [22]. The selected B^\pm mass range is 5.05–5.65 GeV.

Because definitions of forward and backward are tied directly to $\text{sgn}(\eta_B)$, the ambiguous region near $\eta_B = 0$ is given special consideration. We compare η of the B^\pm mesons and their parent b quarks at the production and reconstruction levels in MC@NLO. Rejecting events with $|\eta_B| < 0.1$ removes all B^\pm mesons reconstructed with incorrect q_{FB} without significantly affecting $A_{\text{FB}}(B^\pm)$. After the cut, more than 99.9% of B^\pm mesons give the same q_{FB} as the parent b quark, indicating minimal hadronization effects on $A_{\text{FB}}(B^\pm)$. The distribution of $(\eta_b - \eta_B)$ has a rms width of 0.11.

Background rejection is improved using a boosted decision tree (BDT) [23] trained on a simulated MC signal sample and a background sample from data sidebands around the selected B^\pm mass range (4.0–5.05 and 5.65–7.0). Leading-order signal MC events are generated with PYTHIA [24] and processed through the same reconstruction

code used for data. We weight MC events so that the p_T distributions of the muons match the distributions in data, which are affected by trigger inefficiencies. Additional weights are applied to match distributions of $p_T(B^\pm)$, $p_T(K^\pm)$, and χ^2 of the B^\pm decay vertex fit to data distributions. Finally, we weight MC events so that the probability of reconstructing isolated muons or B^\pm candidates matches the probability measured in data. Isolated particles have no other tracks in a cone of size $\Delta\mathcal{R} = 1$ around them, where $\Delta\mathcal{R} = \sqrt{\Delta\phi^2 + \Delta\eta^2}$ is the angular separation between tracks. This weighting gives optimal agreement between data and simulation in all 40 BDT input variables, which include particle momenta, distances from the $p\bar{p}$ vertex, decay lengths, pointing angles, isolation of the muons and B^\pm meson, and azimuthal angle separation for various particle pairs. A cut on the BDT discriminant is chosen to minimize the statistical uncertainty of $A_{\text{FB}}(B^\pm)$. After all cuts we find one B^\pm candidate in 98.5% of events, with the remainder having two or more candidates. All candidates are used independently in this analysis.

We extract $A_{\text{FB}}(B^\pm)$ from a maximum likelihood fit incorporating a signal probability distribution and three background distributions (see below), which are functions of the reconstructed B^\pm mass $m_{J/\psi K}$ and the kaon energy E_K . The signal distribution $S(m_{J/\psi K}, E_K)$ is modeled by a double-Gaussian function with six parameters, where both Gaussians have the same mean but different widths. The widths have an exponential dependence on E_K . Signal parameters are allowed to differ for the $\eta < -0.1$ and $\eta > 0.1$ regions to account for slight differences in the magnetic field along the beam direction.

The background distribution $P(m_{J/\psi K}, E_K)$ describes $B^\pm \rightarrow J/\psi \pi^\pm$ events where the pion is assigned the kaon mass, creating an artificially high reconstructed B^\pm mass. Distribution P is a reflection of S with the mean mass value shifted to account for the K/π mass difference and the widths scaled by a ratio of the mean mass values. Background distribution $T(m_{J/\psi K})$ describes partially reconstructed decays of type $B_x \rightarrow J/\psi h^\pm X$, which have reconstructed mass lower than the B^\pm mass. Distribution T is empirically modeled using a threshold function with a floating inflection point and the slope fixed from MC simulation [25,26]. Finally, the background distribution $E(m_{J/\psi K}, E_K)$ describes a combinatoric background and is modeled using an exponential function with three parameters, where the slope depends on E_K .

The unbinned fit minimizes LLH, the negative log of the likelihood function \mathcal{L}_n summed over N selected B^\pm candidates, each with weight w_n (defined below):

$$\text{LLH} = -2 \sum_{n=1}^N w_n \ln(\mathcal{L}_n). \quad (2)$$

Here \mathcal{L}_n is a function of the four probability density distributions, with each assigned sample fraction f_i and

forward-backward asymmetry A_i . While systematic effects were studied, the A_i parameters were blinded by adding unknown random offsets. The likelihood \mathcal{L}_n has 26 parameters and is normalized to 1:

$$\mathcal{L}_n = \alpha(E_K)[f_S(1 + q_{\text{FB}}A_S)S + f_P(1 + q_{\text{FB}}A_P)P + f_T(1 + q_{\text{FB}}A_T)T] + f_E(1 + q_{\text{FB}}A_E)E, \quad (3)$$

where $f_E = [1 - \alpha(E_K)(f_S + f_P + f_T)]$ and $\alpha(E_K)$ uses three parameters to describe the dependence of the sample fractions on E_K [25].

Asymmetries in the detector material and J/ψ or K^\pm reconstruction between $\eta < 0$ (the ‘‘north’’ side of the detector) and $\eta > 0$ (the ‘‘south’’ side) can result in an apparent A_{FB} . A north-south asymmetry is defined as $A_{\text{NS}} = (N_N - N_S)/(N_N + N_S)$. Because B^+ and B^- particles on the same side of the detector have opposite q_{FB} , corrections for north-south efficiency differences will generally cancel when determining $A_{\text{FB}}(B^\pm)$. We measure A_{NS} in data samples with no expected production asymmetries. Decays of $\phi \rightarrow K^+K^-$ are used to measure $A_{\text{NS}}(K^\pm)$. Signal and background models are determined from MC simulation and a χ^2 minimization fit is performed simultaneously on north- and south-side data. We measure $A_{\text{NS}}(K^\pm)$ in bins of leading kaon $|\eta|$; there is no significant dependence on p_T . Integrated over all $|\eta|$, $A_{\text{NS}}(K^+) = (0.39 \pm 0.22)\%$ and $A_{\text{NS}}(K^-) = (0.64 \pm 0.23)\%$.

We measure $A_{\text{NS}}(J/\psi)$ using prompt $J/\psi \rightarrow \mu^+\mu^-$ decays. J/ψ mesons with significant L_{xy} are generally from B decays which could exhibit a north-south asymmetry due to $A_{\text{FB}}(B^\pm)$. To reduce the fraction of nonprompt J/ψ mesons to a negligible level we require the J/ψ L_{xy} significance to be less than 1.5. Background events under the peak from 2.9–3.3 GeV are removed with a sideband subtraction, and $A_{\text{NS}}(J/\psi)$ is calculated in bins of $|\eta|$ and p_T . Integrated over all $|\eta|$ and p_T , $A_{\text{NS}}(J/\psi) = (-0.41 \pm 0.04)\%$.

Measured A_{NS} values are used to determine ‘‘efficiency weights’’ w_{K^\pm} and $w_{J/\psi}$ that equalize the relative reconstruction efficiencies on both sides of the detector. Applying these weights has a small effect on $A_{\text{FB}}(B^\pm)$: a shift of 0.06% from w_{K^\pm} and a shift of -0.01% from $w_{J/\psi}$. Uncertainties on $A_{\text{NS}}(J/\psi)$ and $A_{\text{NS}}(K^\pm)$ contribute an uncertainty of 0.003% to $A_{\text{FB}}(B^\pm)$, determined using an ensemble test with 500 Gaussian variations of the A_{NS} values.

The total event weight is $w_n = w_{\text{magnet}}w_{K^\pm}w_{J/\psi}$, where w_{magnet} equalizes the number of events in eight settings of solenoid polarity, toroid polarity, and B^\pm charge. Equalizing the contribution from each magnet polarity combination removes tracking charge asymmetries to first order, since in one polarity a B^+ is reconstructed with the same sign of curvature as a B^- in the opposite polarity. Also equalizing the number of B^+ and B^- candidates eliminates

the need to correct for different K^+ and K^- interaction cross sections in the detector [27].

The weighted data sample contains 160 360 B^\pm candidates and the fit yields $89\,328 \pm 349 B^\pm \rightarrow J/\psi K^\pm$ decays. Although the fit was unbinned, to visualize the data and fit quality, binned distributions of invariant mass $M(J/\psi K)$ for the sum and the difference in the numbers of forward and backward B^\pm candidates with their projected fits are shown in Figs. 1 and 2. Over both mass distributions we obtain $\chi^2/\text{ndf} = 249/214$. We measure a signal asymmetry consistent with zero: $A_{\text{FB}}(B^\pm) = [-0.24 \pm 0.41 (\text{stat})]\%$. The asymmetry is consistent over time and with B^+ and B^- samples fitted separately. Asymmetries of the background distributions are also consistent with zero.

To determine systematic uncertainties on $A_{\text{FB}}(B^\pm)$ a number of variations are made to the analysis. Data sample variations include training four alternative BDTs with different variables or input samples and using a range of BDT discriminant cuts. Fit variations include varying the B^\pm mass range, removing dependences on E_K from the distributions, allowing the slope of $T(m_{J/\psi K})$ to float, and fixing the background asymmetry parameters to zero.

To estimate the systematic error from the reconstruction asymmetries we measure $A_{\text{NS}}(J/\psi)$ and $A_{\text{NS}}(K^\pm)$ using alternate data samples and calculations in different bins or with alternate fit parameters. Biases in the fitting procedure are explored with ensemble tests on randomized data, comparing input and fitted values of $A_{\text{FB}}(B^\pm)$. No bias is observed, and a systematic uncertainty is assigned based on the spread of results in the ensemble test. The total

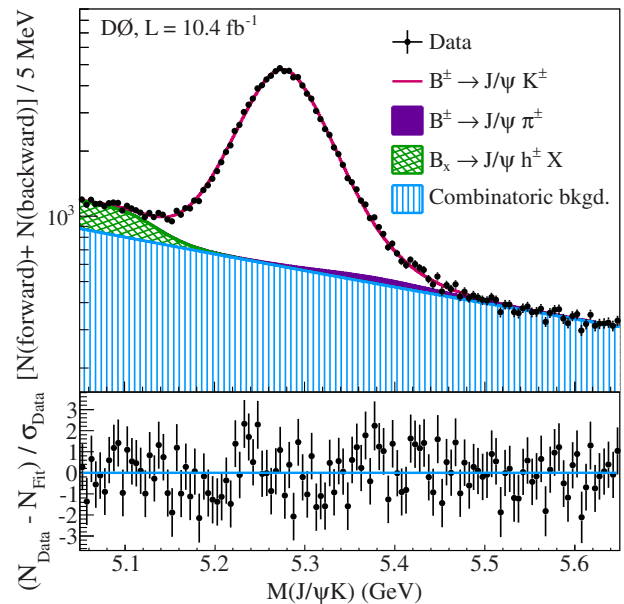


FIG. 1 (color online). Invariant mass $M(J/\psi K)$ of (forward + backward) events with fitted distributions. The lower pane shows the residuals.

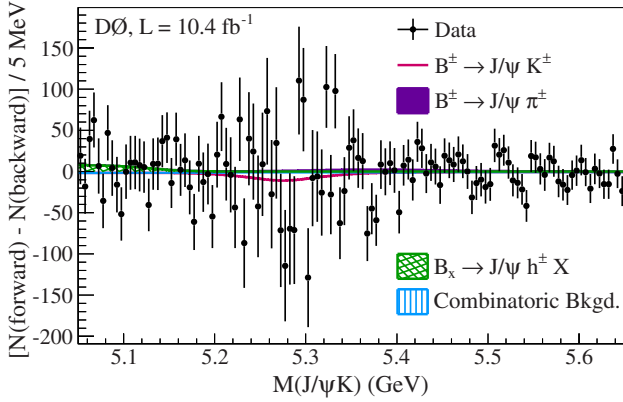


FIG. 2 (color online). Invariant mass $M(J/\psi K)$ of (forward – backward) events with fitted distributions which include the asymmetry parameters A_i .

systematic uncertainty on the data measurement is 0.19%, as summarized in Table I.

To compare this measurement to the SM, the MC@NLO simulation is analyzed as described above, applying $B^\pm \rightarrow J/\psi K^\pm$ selections and weights to correct for muon trigger effects. Additionally, reconstructed muon and kaon tracks must match tracks from generated $B^\pm \rightarrow J/\psi K^\pm$ decays. Since matching reconstructed and generated B^\pm mesons leaves no background events, $A_{\text{FB}}^{\text{SM}}(B^\pm)$ is calculated directly according to Eq. (1).

The dominant systematic uncertainty on $A_{\text{FB}}^{\text{SM}}(B^\pm)$ is due to renormalization and factorization energy scale choices. MC@NLO defines μ_R and μ_F for renormalization and factorization energy scales [15] as the square root of the average of $m_T^2 = m^2 + p_T^2$ for the b and \bar{b} quarks [28], with b quark mass m set to 4.75 GeV. Since $A_{\text{FB}}^{b\bar{b}}$ is zero at leading order, there is a large scale dependence in predictions at next-to-leading order [29]. Both scales are varied independently from $\frac{1}{2}\mu_{R,F}$ to $2\mu_{R,F}$ to estimate an uncertainty due to uncalculated higher orders. Half the largest spread of variations gives a systematic uncertainty of 0.44%. The uncertainty on $A_{\text{FB}}^{\text{SM}}(B^\pm)$ due to b quark fragmentation is estimated by weighting events so the distribution of $p(B^\pm)_\parallel/p(b)$ matches a Bowler function [30] tuned to LEP data or SLD data, where $p(B^\pm)_\parallel$ is the component of

TABLE I. Summary of uncertainties on $A_{\text{FB}}(B^\pm)$ in data.

Source	Uncertainty
Statistical	0.41%
Alternative BDTs and cuts	0.17%
Fit variations	0.06%
Reconstruction asymmetries	0.05%
Fit bias	0.02%
Systematic uncertainty	0.19%
Total uncertainty	0.45%

$p(B^\pm)$ in the b quark direction. Half the largest spread of variations to $A_{\text{FB}}^{\text{SM}}(B^\pm)$ is 0.25%. The negligible PDF uncertainty of 0.03% is calculated by varying the twenty CTEQ6M1 eigenvectors by their uncertainties and determining the standard deviation of the variations. We find $A_{\text{FB}}^{\text{SM}}(B^\pm) = [2.31 \pm 0.34 \text{ (stat)} \pm 0.51 \text{ (syst)}]\%$. Combining all data and MC uncertainties in quadrature, the MC@NLO result differs from data by $(2.55 \pm 0.76)\%$, or 3.3 standard deviations.

Figure 3 shows measurements of $A_{\text{FB}}(B^\pm)$ and $A_{\text{FB}}^{\text{SM}}(B^\pm)$ versus transverse momentum and pseudorapidity. The fully reconstructed $J/\psi K^\pm$ final state produces good kinematic agreement between reconstructed and generated B^\pm mesons, so corrections to recover the true B^\pm kinematics are unnecessary. The average p_T of the B^\pm mesons is 12.9 GeV. We find that $A_{\text{FB}}(B^\pm)$ is systematically lower than $A_{\text{FB}}^{\text{SM}}(B^\pm)$ for all pseudorapidities, and for $p_T(B) = 9\text{--}30$ GeV. Considering the MC systematic uncertainties to be correlated (uncorrelated), Fig. 3(a) has $\chi^2 = 10.3$ (11.8) for three bins and Fig. 3(b) has $\chi^2 = 6.6$ (7.0) for seven bins.

In conclusion, we have measured the forward-backward asymmetry in the production of B^\pm mesons with $B^\pm \rightarrow J/\psi K^\pm$ decays in $p\bar{p}$ collisions at $\sqrt{s} = 1.96$ TeV.

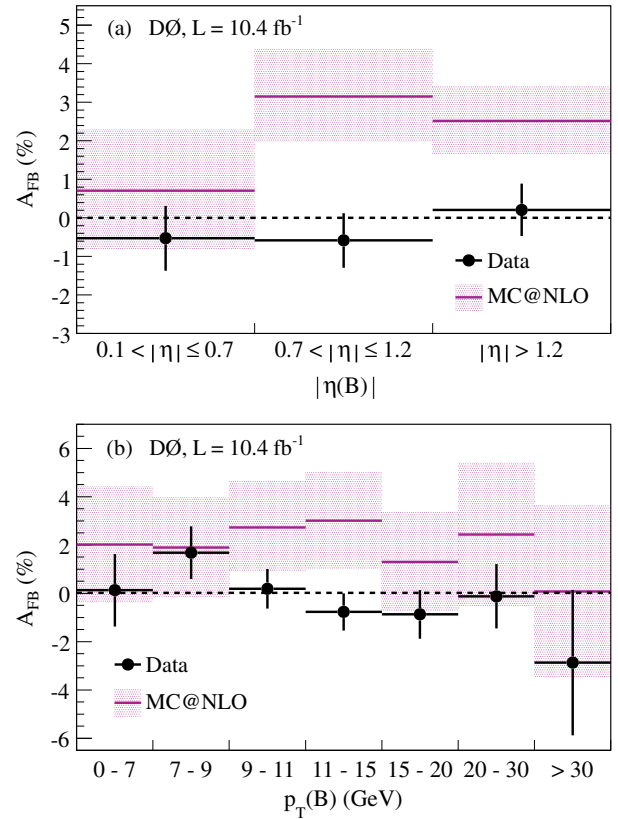


FIG. 3 (color online). Comparison of $A_{\text{FB}}(B^\pm)$ and $A_{\text{FB}}^{\text{SM}}(B^\pm)$ in bins of (a) $|\eta_B|$ and (b) $p_T(B)$. Data points and MC bands include statistical uncertainties convoluted with systematic uncertainties.

For B^\pm mesons with a mean p_T of 12.9 GeV, the result is $A_{\text{FB}}(B^\pm) = [-0.24 \pm 0.41 \text{ (stat)} \pm 0.19 \text{ (syst)}]\%$, which is the first measurement of this quantity. The observed discrepancy of ≈ 3 standard deviations between our measurement and the MC@NLO estimate suggests that more rigorous determination of the standard model prediction is needed to interpret these results.

We thank the staffs at Fermilab and collaborating institutions, and acknowledge support from the Department of Energy and National Science Foundation (United States of America); Alternative Energies and Atomic Energy Commission and National Center for Scientific Research/National Institute of Nuclear and Particle Physics (France); Ministry of Education and Science of the Russian Federation, National Research Center “Kurchatov Institute” of the Russian Federation, and Russian Foundation for Basic Research (Russia); National Council for the Development of Science and Technology and Carlos Chagas Filho Foundation for the Support of Research in the State of Rio de Janeiro (Brazil); Department of Atomic Energy and Department of Science and Technology (India); Administrative Department of Science, Technology and Innovation (Colombia); National Council of Science and Technology (Mexico); National Research Foundation of Korea (Korea); Foundation for Fundamental Research on Matter (The Netherlands); Science and Technology Facilities Council and The Royal Society (United Kingdom); Ministry of Education, Youth and Sports (Czech Republic); Bundesministerium für Bildung und Forschung (Federal Ministry of Education and Research) and Deutsche Forschungsgemeinschaft (German Research Foundation) (Germany); Science Foundation Ireland (Ireland); Swedish Research Council (Sweden); China Academy of Sciences and National Natural Science Foundation of China (China); and Ministry of Education and Science of Ukraine (Ukraine).

^aVisitor from Augustana College, Sioux Falls, SD, USA.

^bVisitor from The University of Liverpool, Liverpool, UK.

^cVisitor from DESY, Hamburg, Germany.

^dVisitor from Universidad Michoacana de San Nicolas de Hidalgo, Morelia, Mexico.

^eVisitor from SLAC, Menlo Park, CA, USA.

^fVisitor from University College London, London, UK.

^gVisitor from Centro de Investigacion en Computacion - IPN, Mexico City, Mexico.

^hVisitor from Universidade Estadual Paulista, São Paulo, Brazil.

ⁱVisitor from Karlsruher Institut für Technologie (KIT) - Steinbuch Centre for Computing (SCC), D-76128 Karlsruhe, Germany.

^jVisitor from Office of Science, U.S. Department of Energy, Washington, D.C. 20585, USA.

^kVisitor from American Association for the Advancement of Science, Washington, D.C. 20005, USA.

^lVisitor from Kiev Institute for Nuclear Research, Kiev, Ukraine.

^mVisitor from University of Maryland, College Park, Maryland 20742, USA.

ⁿVisitor from European Organization for Nuclear Research (CERN), Geneva, Switzerland.

- [1] L. G. Almeida, G. Sterman, and W. Vogelsang, *Phys. Rev. D* **78**, 014008 (2008); J. H. Kühn and G. Rodrigo, *J. High Energy Phys.* **01** (2012) 063; J. A. Aguilar-Saavedra, D. Amidei, A. Juste, and M. Perez-Victoria arXiv:1406.1798.
- [2] V. M. Abazov *et al.* (D0 Collaboration), *Phys. Rev. D* **84**, 112005 (2011).
- [3] T. Aaltonen *et al.* (CDF Collaboration), *Phys. Rev. D* **83**, 112003 (2011); **87**, 092002 (2013); **88**, 072003 (2013).
- [4] M. I. Gresham, I.-W. Kim, and K. M. Zurek, *Phys. Rev. D* **83**, 114027 (2011); J. A. Aguilar-Saavedra and M. Perez-Victoria, *J. High Energy Phys.* **09** (2011) 097; J. F. Kamenik, J. Shu, and J. Zupan, *Eur. Phys. J. C* **72**, 2102 (2012).
- [5] B. Grinstein and C. W. Murphy, *Phys. Rev. Lett.* **111**, 062003 (2013); **112**, 239901(E) (2014).
- [6] S. Ipek, *Phys. Rev. D* **87**, 116010 (2013).
- [7] V. M. Abazov *et al.* (D0 Collaboration), *Phys. Rev. D* **87**, 011103(R) (2013); **88**, 112002 (2013); **90**, 072011 (2014).
- [8] W. Bernreuther and Z.-G. Si, *Phys. Rev. D* **86**, 034026 (2012); M. Czakon, P. Fiedler, and A. Mitov, arXiv:1411.3007.
- [9] S. Chatrchyan *et al.* (CMS Collaboration), *J. High Energy Phys.* **04** (2014) 191.
- [10] G. Aad *et al.* (ATLAS Collaboration), *J. High Energy Phys.* **02** (2014) 107.
- [11] R. Aaij *et al.* (LHCb Collaboration), *Phys. Rev. Lett.* **113**, 082003 (2014).
- [12] J. H. Kühn and G. Rodrigo, *Phys. Rev. D* **59**, 054017 (1999).
- [13] The D0 collaboration defines a coordinate system with the z axis along the proton beam direction, the x axis pointing away from the Tevatron center, and the y axis pointing upwards. Pseudorapidity is defined as $\eta = -\ln[\tan(\theta/2)]$, where θ is the laboratory frame polar angle. Angle ϕ is the azimuthal angle in the x - y plane.
- [14] A. V. Manohar and M. Trott, *Phys. Lett. B* **711**, 313 (2012).
- [15] S. Frixione and B. R. Webber, *J. High Energy Phys.* **06** (2002) 029; S. Frixione, P. Nason, and B. R. Webber, *J. High Energy Phys.* **08** (2003) 007.
- [16] J. Pumplin, D. R. Stump, J. Huston, H.-L. Lai, P. Nadolsky, and W.-K. Tung, *J. High Energy Phys.* **07** (2002) 012; D. Stump, J. Huston, J. Pumplin, W.-K. Tung, H.-L. Lai, S. Kuhlmann, and J. Francis Owens, *J. High Energy Phys.* **10** (2003) 046.
- [17] G. Corcella *et al.*, *J. High Energy Phys.* **01** (2001) 010.
- [18] R. Brun and F. Carminati CERN Program Library Writeup W5013, 1993. We use GEANT version 3.15.
- [19] V. M. Abazov *et al.* (D0 Collaboration), *Nucl. Instrum. Methods A* **565**, 463 (2006).
- [20] V. M. Abazov *et al.*, *Nucl. Instrum. Methods A* **552**, 372 (2005); V. M. Abazov *et al.* (D0 Collaboration), *Nucl. Instrum. Methods A* **737**, 281 (2014).

- [21] The pointing angle is defined as the angle between a particle's momentum vector and the vector from the $p\bar{p}$ vertex to the particle's decay vertex, with vectors defined in the x - y plane.
- [22] K. A. Olive *et al.* (Particle Data Group), *Chin. Phys. C* **38**, 090001 (2014).
- [23] A. Hoecker *et al.* Toolkit for multivariate data analysis, *Proc. Sci. ACAT* (2007) 040. We use version 4.1.0.
- [24] T. Sjöstrand, S. Mrenna, and P. Skands, *J. High Energy Phys.* **05** (2006) 026.
- [25] V. M. Abazov *et al.* (D0 Collaboration), *Phys. Rev. Lett.* **110**, 241801 (2013).
- [26] V. M. Abazov *et al.* (D0 Collaboration), *Phys. Rev. D* **87**, 072006 (2013).
- [27] V. M. Abazov *et al.* (D0 Collaboration), *Phys. Rev. D* **86**, 072009 (2012); **82**, 032001 (2010).
- [28] S. Frixione (private communication).
- [29] J. M. Campbell and R. K. Ellis Report No. FERMILAB-PUB-12-078-T (2012).
- [30] G. Corcella and V. Drollinger, *Nucl. Phys.* **B730**, 82 (2005).